Spectroscopic properties and continuous-wave laser operation of Nd:Ca 0.7 La 0.3 Mg 0.3 Al 11.7 O 19 crystal

Yuxin Pan, Bei Liu, Jian Liu, Qingsong Song, Jie Xu, Dongzhen Li, Peng Liu, Jie Ma, Xiaodong Xu, Hui Lin, et al.

Research Article | Vol. 10, No. 5 / 1 May 2020 / Optical Materials Express 1255
Optical Materials EXPRESS

Spectroscopic properties and continuous-wave laser operation of Nd:$Ca_{0.7}La_{0.3}Mg_{0.3}Al_{11.7}O_{19}$ crystal

YUXIN PAN,[1,2] BEI LIU,[1] JIAN LIU,[3] QINGSONG SONG,[1] JIE XU,[1] DONGZHEN LI,[1] PENG LIU,[1] JIE MA,[1] XIAODONG XU,[1,5] HUI LIN,[2] JUN XU,[3,6] AND KHEIRREDDINE LEBBOU[4]

[1]*Jiangsu Key Laboratory of Advanced Laser Materials and Devices, School of Physics and Electronic Engineering, Jiangsu Normal University, Xuzhou 221116, China*
[2]*Engineering Research Center of Optical Instrument and System, Ministry of Education and Shanghai Key Lab of Modern Optics and Systems, University of Shanghai for Science and Technology, Shanghai 200093, China*
[3]*School of Physics Science and Engineering, Institute for Advanced Study, Tongji University, Shanghai 200092, China*
[4]*Institut Lumière Matière, UMR5306 Université Lyon1-CNRS, Université de Lyon, Lyon 69622, Villeurbanne Cedex, France*
[5]*xdxu79@jsnu.edu.cn*
[6]*xujun@mail.shcnc.ac.cn*

Abstract: The polarized absorption spectra, polarized fluorescence spectra and fluorescence decay curve of Nd:$Ca_{0.7}La_{0.3}Mg_{0.3}Al_{11.7}O_{19}$ (CL*n*A) crystal were recorded at room temperature. The Judd-Ofelt parameters Ω_2, Ω_4 and Ω_6 were calculated to be 0.80×10^{-20} cm^2, 3.83×10^{-20} cm^2 and 2.71×10^{-20} cm^2, respectively. The spontaneous transition rates, branching ratios and the radiative lifetime were calculated for the $^4F_{3/2}$ excited state. The emission cross section is 4.01×10^{-20} cm^2 at 1052 nm for σ-polarization and 0.96×10^{-20} cm^2 at 1052 nm for π-polarization, respectively. Continuous-wave (CW) laser operations of a-cut and c-cut Nd:$Ca_{0.7}La_{0.3}Mg_{0.3}Al_{11.7}O_{19}$ crystals have been demonstrated.

1. Introduction

Nd^{3+}-doped laser crystals provide an efficient way to generate high-power and low-threshold laser around 1 μm, which can be applied in various fields including medicine, industry, military and scientific researches [1–3]. Compared with Yb^{3+}-doped crystals, Nd^{3+}-doped crystals have relative narrow emission band-width, which limits the application in ultra-short pulse generation [4]. However, Nd^{3+}-doped disordered crystals are promising in realizing ultrafast mode-locked laser due to the inhomogeneous broadening of the emission spectra. Up to now, a great deal of Nd^{3+} lasers has been developed based on various host disordered crystals, such as CNGG [5], CLNGG [6], $CaYAlO_4$ [7], $CaGdAlO_4$ [8], $Y_3ScAl_4O_{12}$ [9], $Ca_2Ga_2SiO_7$ [10], $LaMgAl_{11}O_{19}$ [11], $Sr_{0.7}La_{0.3}Mg_{0.3}Al_{11.7}O_{19}$ [12], $SrLaGa_3O_7$ [13], $Ca_3La_2(BO_3)_4$ [14] and so on.

Nd^{3+}-doped calcium-lanthanum-aluminate (Nd:$Ca_{1-x}La_xMg_xAl_{12-x}O_{19}$, CL*n*A), which is formed from calcium ($CaAl_{12}O_{19}$) and lanthanide ($LaMgAl_{11}O_{19}$) hexaaluminates, has a magnetoplumbite structure $PbFe_{12}O_{19}$ (space group $P6_3/mmc$) where Mg^{2+} ions substitute for Al^{3+} ions for charge compensation [15,16]. In CL*n*A crystal, Nd^{3+} ions are occupied in two different sites, which leads to inhomogeneous broadening of the fluorescence spectra. In 1988, Gbehi *et al*. [15] reported the growth of CL*n*A crystal using the melting zone technique and found that the fluorescence spectra of CL*n*A crystal and Nd:$LaMgAl_{11}O_{19}$ crystal are very similar. However, no any detailed report about the polarized spectral properties can be found in [15].

#389014 https://doi.org/10.1364/OME.389014
Journal © 2020 Received 23 Jan 2020; revised 2 Apr 2020; accepted 7 Apr 2020; published 16 Apr 2020

Optical Materials EXPRESS

In this paper, we studied the polarized absorption and emission spectra of CL*n*A crystal. Using Judd-Ofelt theory, the spectral parameters of Nd^{3+} ions in CL*n*A crystal were obtained. The CW laser operation of CL*n*A crystal was demonstrated by LD pumping.

2. Experiments

The CL*n*A crystal was grown by the Czochralski method. On the basis of spectral properties previously performed on Nd:$LaMgAl_{11}O_{19}$ [17] and Nd:$Sr_{0.7}La_{0.3}Mg_{0.3}Al_{11.7}O_{19}$ [18] crystals, the Nd^{3+} concentration of 5 at.% has been selected in CL*n*A crystal. High purity (>99.999%) La_2O_3, MgO, $CaCO_3$, Al_2O_3 and Nd_2O_3 powders were used as raw materials. They were dried and weighed according to the formula $Ca_{0.7}La_{0.25}Nd_{0.05}Mg_{0.3}Al_{11.7}O_{19}$. After the compounds were ground and thoroughly mixed, they were pressed into pieces and then sintered at 1300 °C for 24 h in the air. The charge was loaded into an iridium crucible for crystal growth. A $LaMgAl_{11}O_{19}$ crystal with a <100> orientation was used as the seed.

The crystal sample for spectroscopic measurements was cut from the as-grown CL*n*A crystal, and the surfaces perpendicular to the <100> growth axis were polished. The Nd^{3+} ions concentration in the sample was 1.44×10^{-20} ions/cm^{3}. The polarized absorption spectra was measured by a UV–VIS–NIR spectrophotometer (Model Cary-5000, Varian, USA) with a spectral interval of 1 nm at room temperature. The fluorescence spectra with a spectral interval of 0.5 nm, as well as the decay curve of the $^4F_{3/2}$ multiplet, were recorded using a FLS980 spectrometer (Edinburgh) under 796 nm excitation. All the measurements were taken at room temperature.

Laser experimental setup of LD-pumped continuous-wave CL*n*A crystal lasers is shown schematically in Fig. 1. Two laser gain media were CL*n*A crystals cut along *a* and *c* crystalline axis with dopant concentration of 5% and dimensions of $3 \times 3 \times 6$ mm^3. The pump source in our experiment was a fiber-coupled laser diode (LD) centered around 800 nm with a core diameter of about 200 μm and a numerical aperture of 0.22. The pump light delivered from the fiber was firstly paralleled by a convex lens with focal length of 50 mm, and then was focused into the laser crystal with a spot radius of ~150 μm by a f = 150 mm convex lens. The input mirror M1 was coated with high reflectivity for laser wavelength and high transmission for the pump light. Three different output couplers (OCs), with transmissions of 5%, 10% and 15% at 1053 nm, were used in the experiments. The cavity length was about 15 mm.

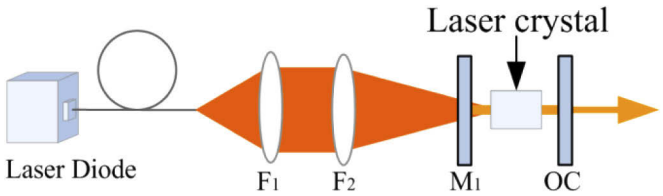

Fig. 1. The schematic of laser experimental setup of a diode-pumped CL*n*A lasers.

3. Results and discussion

The polarized absorption cross section spectra of CL*n*A crystal in the wavelength region of 300-1000 nm were recorded at room temperature and shown in Fig. 2. Nine absorption bands are corresponding to transitions from the ground state $^4I_{9/2}$ to the various excited states of Nd^{3+} ions. Owing to the anisotropy of the crystal, the absorption spectra show strong polarization dependence and the σ-polarization absorption cross section is much larger than that of π-polarization. From the Fig. 2, we can see that the prominent absorption peaks around 583, 729, and 792 nm correspond to the transitions of $^4I_{9/2}\rightarrow{}^4G_{5/2}+{}^2G_{7/2}$, $^4I_{9/2}\rightarrow{}^4F_{7/2}+{}^4S_{3/2}$, and $^4I_{9/2}\rightarrow{}^4F_{5/2}+{}^2H_{9/2}$, respectively. The absorption cross-sections were calculated to be

Optical Materials EXPRESS

2.18×10^{-20} cm^2 at 792 nm for σ polarization and 0.40×10^{-20} cm^2 at 795 nm for π polarization, with full width at half maximum (FWHM) of 11.2 nm and 20.4 nm. The absorption cross section for σ polarization is larger than the value of $La_{0.95}Nd_{0.05}MgAl_{11}O_{19}$ (1.7×10^{-20} cm^2 at 795 nm [17]) and $Sr_{0.7}La_{0.25}Nd_{0.05}Mg_{0.3}Al_{11.7}O_{19}$ (8.6×10^{-21} cm^2 at 792 nm [18]). The FWHMs of CL*n*A crystal are larger than that of Nd:$CaGdAlO_4$ crystal (5 nm for σ polarization, 4 nm for π polarization [19]) and Nd:$CaYAlO_4$ crystal (both 5 nm for σ and π polarization [20]). The broad bandwidth means that CL*n*A crystal is more suitable for diode pumping and indicates an inhomogeneous broadening behavior, which is probably due to the disordered structure of CL*n*A crystal.

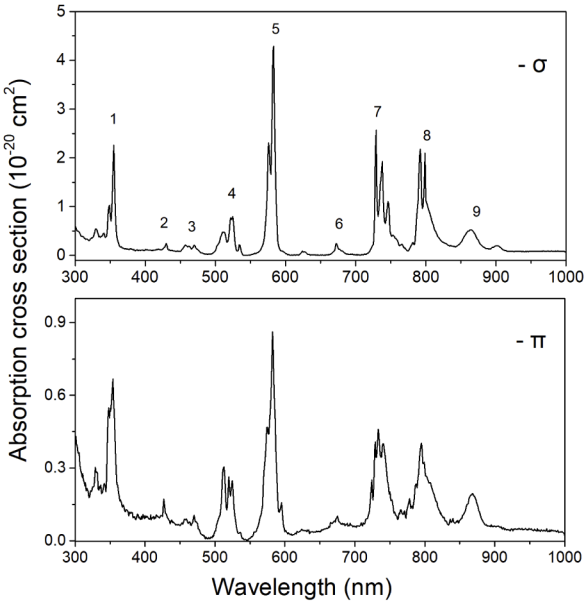

Fig. 2. Polarized absorption cross-sections of CL*n*A crystal at room temperature. (1 - $^2L_{15/2}+^4D_{1/2}+^2I_{11/2}+^4D_{5/2}+^4D_{3/2}$, 2 - $^2P_{1/2}$, 3 - $^2K_{15/2}+^2D_{3/2}+^4G_{11/2}+^2G_{9/2}$, 4 - $^4G_{9/2}+^4G_{7/2}+^2K_{13/2}$, 5 - $^4G_{5/2}+^2G_{7/2}$, 6 - $^4F_{9/2}$, 7 - $^4F_{7/2}+^4S_{3/2}$, 8 - $^2H_{9/2}+^4F_{5/2}$, 9 - $^4F_{3/2}$).

The Judd-Ofelt theory [21,22] was applied to analyze the polarized absorption spectra, and then the branching ratios of the transitions from the upper laser level $^4F_{3/2}$ and the radiative lifetime of the level can be evaluated. The detailed calculation procedures are the same as Ref. [23,24]. The reduced matrix elements used for absorption and emission transitions can be consulted in [23] and [25], respectively. In Table 1, average wavelength of different transition, the line strength of experiment and calculation, and RMS deviation of Nd^{3+} ion in CL*n*A crystal are given. The value of RMS deviations is 0.277×10^{-20} cm^2 and 0.182×10^{-20} cm^2 for σ-polarization and π-polarization, which indicates a good agreement between the experimental and the calculated spectral intensities.

Three J-O intensity parameters of different Nd^{3+} doped crystals are listed in Table 2. For CL*n*A crystal, the effective JO intensity parameters were calculated by $\Omega = (2\Omega_\sigma + \Omega_\pi)/3$, and the $\Omega_{2,4,6}$ were obtained to be 0.80×10^{-20} cm^2, 3.83×10^{-20} cm^2, and 2.71×10^{-20} cm^2, respectively. In general, Ω_2 is related to the chemical bonding, structural change and symmetry of the ligand field around Nd^{3+} ion site. The result indicates that the covalency of CL*n*A is larger than that of Nd:YAG, but lower than that of Nd^{3+} doped $LaMgAl_{11}O_{19}$, $Sr_{0.7}La_{0.3}Mg_{0.3}Al_{11.7}O_{19}$, $LuVO_4$, $Ca_2Ga_2SiO_7$ and $Ca_2Ga_2SiO_7$ crystal. Ω_4/Ω_6 is the spectroscopic quality factor which depends

Optical Materials EXPRESS

Table 1. The average wavelength of different transition, the line strength of experiment and calculation, and RMS deviation of Nd^{3+} ion in CL*n*A crystal

Excited state	σ-polarization			π-polarization		
	$\bar{\lambda}$(nm)	S_{exp} (10^{-20} cm^2)	S_{cal} (10^{-20} cm^2)	$\bar{\lambda}$(nm)	S_{exp} (10^{-20} cm^2)	S_{cal} (10^{-20} cm^2)
$^2L_{15/2}$+$^4D_{1/2}$+$^2I_{11/2}$+$^4D_{5/2}$+$^4D_{3/2}$	347	3.079	2.830	347	1.318	1.144
$^2P_{1/2}$	429	0.087	0.174	432	0.085	0.074
$^2K_{15/2}$+$^2D_{3/2}$+$^4G_{11/2}$+$^2G_{9/2}$	465	0.532	0.346	464	0.291	0.113
$^4G_{9/2}$+$^4G_{7/2}$+$^2K_{13/2}$	518	1.646	1.584	517	0.637	0.527
$^4G_{5/2}$+$^2G_{7/2}$	580	4.192	4.199	580	1.313	1.297
$^4F_{9/2}$	675	0.194	0.199	687	0.029	0.046
$^4F_{7/2}$+$^4S_{3/2}$	740	2.961	2.671	738	0.688	0.532
$^2H_{9/2}$+$^4F_{5/2}$	800	2.673	3.082	797	0.669	0.836
$^4F_{3/2}$	869	0.970	1.291	866	0.228	0.497
RMS (10^{-20} cm^2)		0.277			0.182	

on the rigidity of the host matrix [29]. The spectroscopic quality Ω_4/Ω_6 of CL*n*A crystal is 1.41 (more than 1), suggesting that CL*n*A crystal is a promising medium for efficient laser operation.

Table 2. The J-O intensity parameters of different Nd3+ doped crystals.

Crystals		Ω_2	Ω_4	Ω_6	Ref.
$LaMgAl_{11}O_{19}$		1.21	3.63	2.35	[17]
$Sr_{0.7}La_{0.3}Mg_{0.3}Al_{11.7}O_{19}$		0.87	1.55	0.95	[18]
YAG		0.62	1.70	5.76	[26]
$LuVO_4$		7.18	5.99	5.78	[27]
$Ca_2Ga_2SiO_7$		1.12	2.87	2.72	[28]
CL*n*A	Ω_σ	1.16	4.74	3.72	This work
	Ω_π	0.06	2.01	0.67	
	Ω	0.80	3.83	2.71	

Intensity parameter	Ω (10^{-20} cm^2)		
	σ-polarization	π-polarization	Ω= $(2\Omega_\sigma + \Omega_\pi)/3$
Ω_2	1.16	0.06	0.80
Ω_4	4.74	2.01	3.83
Ω_6	3.72	0.67	2.71

Based on the obtained intensity parameters, the calculated radiative transition rates, branching ratios and the radiative lifetimes of $^4F_{3/2}\rightarrow{}^4I_{9/2}$, $^4F_{3/2}\rightarrow{}^4I_{11/2}$, $^4F_{3/2}\rightarrow{}^4I_{13/2}$ and $^4F_{3/2}\rightarrow{}^4I_{15/2}$ transitions of CL*n*A crystal are given in Table 3. We can see that the branching ratio of the $^4F_{3/2}\rightarrow{}^4I_{9/2}$ transition is larger than that of the $^4F_{3/2}\rightarrow{}^4I_{11/2}$ transition for each polarization. The radiative lifetime of $^4F_{3/2}$ energy level was calculated to be 364 μs, which is smaller than the value of $La_{0.95}Nd_{0.05}MgAl_{11}O_{19}$ (401 μs [17]) and $Sr_{0.7}La_{0.25}Nd_{0.05}Mg_{0.3}Al_{11.7}O_{19}$ (500 μs [18]), but much larger than the value of other oxide crystals, such as Nd:$CaNb_2O_6$ (167 μs [30]), Nd:$CaYAlO_4$ (114 μs [20]), Nd:$Bi_4Ge_3O_{12}$ (293 μs [31]) and Nd:$GdNbO_4$ (194 μs [32])). The results indicate that CL*n*A crystal owns a higher energy storage ability.

The polarized fluorescence spectra of the CL*n*A crystal in the range of 850-1450 nm were measured under 796 nm excitation. The stimulated emission cross section, which is one of the

Optical Materials EXPRESS

Table 3. Calculated radiative transition rates, branching ratios, radiative lifetimes for different transition levels of CL*n*A crystal.

Transitions	σ-polarization		π-polarization	
	A_σ (S^{-1})	β_σ (%)	A_π (S^{-1})	β_π (%)
$^4F_{3/2}\rightarrow{}^4I_{9/2}$	1698.31	47.50	643.69	59.58
$^4F_{3/2}\rightarrow{}^4I_{11/2}$	1579.44	44.17	383.63	35.51
$^4F_{3/2}\rightarrow{}^4I_{13/2}$	291.67	8.16	51.98	4.81
$^4F_{3/2}\rightarrow{}^4I_{15/2}$	6.19	0.17	1.11	0.10
Radiative lifetime (μs)		364		

most important parameters affecting the potential laser performance, can be calculated from the fluorescence spectra using the Füchtbauere Ladenburg (F–L) formula [33], as presented in Fig. 3. Three emission bands centered at 850-940 nm, 1040-1160 nm and 1320-1440 nm are assigned to the transitions of $^4F_{3/2}\rightarrow{}^4I_{9/2}$, $^4F_{3/2}\rightarrow{}^4I_{11/2}$ and $^4F_{3/2}\rightarrow{}^4I_{13/2}$, respectively. The most intense emission appears at 1052 nm and the experimental $^4F_{3/2}\rightarrow{}^4I_{11/2}$ branching ratios were calculated to be 50.64% for σ polarization and 45.78% for π polarization. The intrinsic uncertainty of Judd-Ofelt calculation (±20%) [34] is large enough to explain the deviation observed between the experimental and calculated branching ratios. The calculated emission cross section is 4.01×10^{-20} cm^2 for σ-polarization and 0.96×10^{-20} cm^2 for π-polarization both at 1052 nm, respectively, with FWHM of 7.5 and 7.3 nm. The FWHM is little larger than the value of Nd:$LaMgAl_{11}O_{19}$ (6.6 nm for σ polarization [17]). The broad bandwidth confirms an inhomogeneous broadening behavior, which accounts for the disordered structure of CL*n*A crystal. In 2000, Yang et al. [35] reported a self-mode locked Nd:$LaMgAl_{11}O_{19}$ laser pumped by a laser diode with the transform-limited pulses of 631 fs duration. Considering the spectral parameters of CL*n*A crystal, one can estimate the tunable laser operation with tunable region of tens of nanometers and mode-locked femtosecond laser operation from CL*n*A crystal.

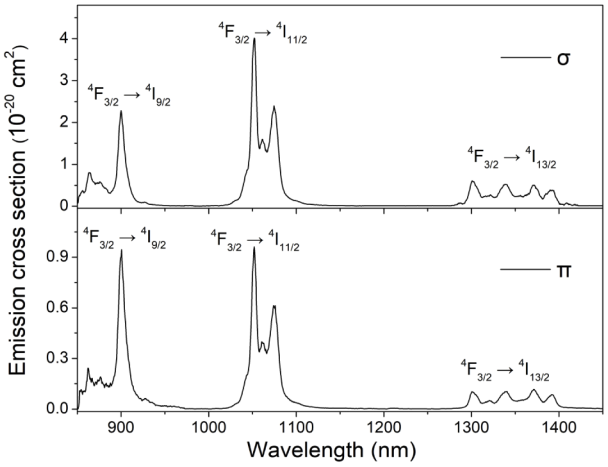

Fig. 3. Polarized emission cross sections of CL*n*A crystal excited by 795 nm at room temperature.

Figure 4 shows the fluorescence decay curve of $^4F_{3/2}$ multiplet. The fluorescence lifetime was calculated to be 333 μs by a single exponential fitting, which is comparable with the value of $La_{0.95}Nd_{0.05}MgAl_{11}O_{19}$ (321 μs [17]), $Sr_{0.7}La_{0.25}Nd_{0.05}Mg_{0.3}Al_{11.7}O_{19}$ (372 μs [18]) and Nd:$SrLaGa_3O_7$ (318 μs [36]) but much longer than that of Nd:YAG (248 μs [37]), Nd:YVO_4 (87

Optical Materials EXPRESS

μs [38]), Nd:$CaGdAlO_4$ (123 μs [19]) and Nd:$CaYAlO_4$ (129 μs [20]). According to the radiative lifetime from J-O theory, the luminescent quantum efficiency of the $^4F_{3/2}$ level was calculated to be 91.5% by the equation of $\eta=\tau/\tau_{rad}$. The results show that CL*n*A crystal is a promising gain medium for solid-state laser generation.

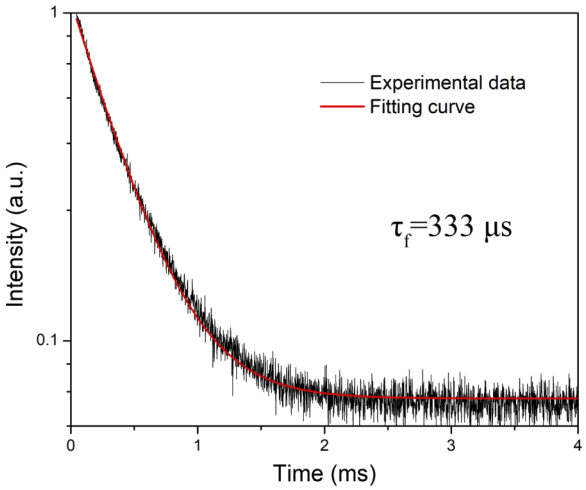

Fig. 4. Room temperature fluorescence decay curve of the $^4F_{3/2}$ manifold of CL*n*A.

The output power characteristics with respect to absorbed pump power of a-cut CL*n*A laser is shown in Fig. 5(a). The highest output power of 5.40 W was obtained with a OC of $T = 5\%$ under the absorbed pump power of 11.51 W, corresponding to an optical-to-optical efficiency of about 46.9% and a slope efficiency of 47.7%. The laser threshold was measured to be 107 mW of absorbed power. When the transmission of output coupler was 10% and 15%, the maximum output power changed to 5.08 W and 4.79 W, while the corresponding slope efficiency became 45.2% and 43.0%, respectively. The maximum output power and slope efficiency of CL*n*A are larger than those of Nd:$LaMgAl_{11}O_{19}$ (1.71 W, 40.4% [17]), but lower than those of Nd:$Sr_{0.7}La_{0.3}Mg_{0.3}Al_{11.7}O_{19}$ (6.9 W, 50% [18]). At maximum, the peak wavelength was measured to be 1052.76 nm (see Fig. 5(b)). There was no pump saturation in our experiments, which indicates the output power can be further scaled with high pump power.

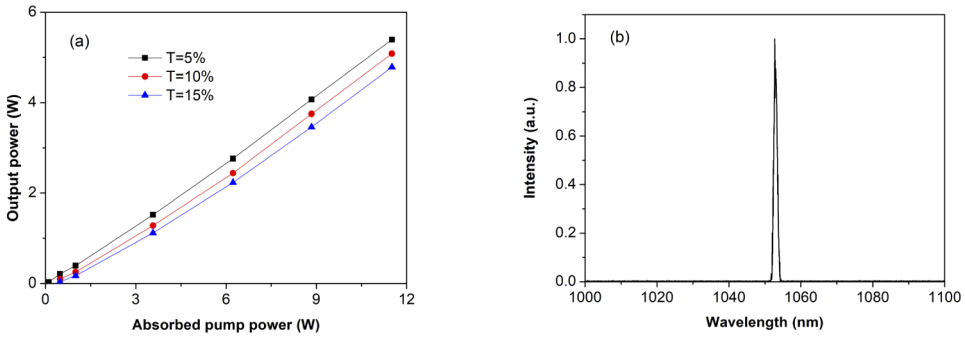

Fig. 5. (a) The dependence of output power on absorbed pump power of a-cut CL*n*A laser and (b) The corresponding laser spectrum with peak at 1052.76 nm.

The experimental results of the c-cut CL*n*A crystal are shown in Fig. 6(a). Using the output coupler with transmission of 10%, a maximum output up to 4.78 W was achieved with threshold

Optical Materials EXPRESS

of 429 mW of absorbed power, which led to a slope efficiency of about 30.5% by linear fit. Using the output coupler with transmission of 15%, the maximum output power decreased to be 4.75 W and the corresponding slope efficiency was linearly fitted to be about 31.2%. Using the output coupler with transmission of 5%, the maximum output power further decreased to be 4.26 W with a slope efficiency of about 27.1%. From the output power curves in Fig. 5(a) and Fig. 6(a), one can find the a-cut CL*n*A crystal has better laser performance than the c-cut CL*n*A crystal. The saturation effect at high pump power of c-cut CL*n*A crystal should be explained by thermal lensing effect inside the c-cut CL*n*A crystal, which led to the laser operation at stability limit or even unstable any more. Figure 6(b) shows the laser wavelength registered at maximum output power with a peak at 1052.84 nm.

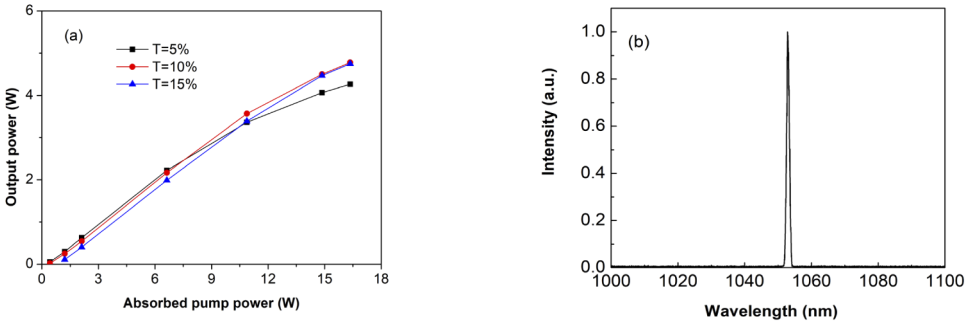

Fig. 6. (a)The dependence of output power on absorbed pump power of c-cut CL*n*A laser and (b) The corresponding laser spectrum with peak at 1052.84 nm.

4. Conclusion

In summary, the polarized absorption spectra, the polarized fluorescence spectra, and the fluorescence decay curve of CL*n*A crystal were recorded at room temperature. The absorption cross-sections are 2.18×10^{-20} cm^2 at 792 nm for σ polarization and 0.40×10^{-20} cm^2 at 795 nm for π polarization with FWHM of 11.2 nm and 20.4 nm. The effective Judd-Ofelt parameters Ω_2, Ω_4 and Ω_6 were calculated to be 0.80×10^{-20} cm^2, 3.83×10^{-20} cm^2 and 2.71×10^{-20} cm^2, respectively. The spontaneous transition rates, branching ratios and the radiative lifetime were calculated for the $^4F_{3/2}$ excited state. The emission cross section is 4.01×10^{-20} cm^2 for σ-polarization and 0.96×10^{-20} cm^2 for π-polarization both at 1052 nm with FWHM of 7.5 and 7.3 nm, respectively. The fluorescence lifetime is 333 μs, and the luminescent quantum efficiency of the $^4F_{3/2}$ level is 70.1%. Continuous-wave laser operation of the a- and c-cut samples under 800 nm laser diode has been demonstrated. Maximum output powers of 5.40 W and 4.78 W were obtained for the a-cut and c-cut samples, corresponding to a slope efficiency of 47.7% and 30.5%, respectively. Improving the laser performance could be realized by optimizing the quality of CL*n*A crystal.

Funding

National Natural Science Foundation of China (61621001).

Disclosures

The authors declare no conflicts of interest.

References

1. T. J. Kane, W. J. Kozlovshy, and R. I. Byer, "Coherent laser radar at 1.06 μm using Nd:YAG lasers," Opt. Lett. **12**(4), 239–241 (1987).

Optical Materials EXPRESS

2. K. Washio, "Neodymium-doped solid-state lasers and their applications to materials processing," Mater. Chem. Phys. **31**(1-2), 57–66 (1992).
3. R. Moncorge, B. Chambon, J. Y. Rivoire, N. Garnier, E. Descroix, P. Laporte, H. Guillet, S. Roy, J. Mareschal, D. Pelenc, J. Doury, and P. Farge, "Nd doped crystals for medical laser applications," Opt. Mater. **8**(1-2), 109–119 (1997).
4. E. Sorokin, M. H. Ober, I. Sorokina, E. Wintner, and A. J. Schmidt, "Femtosecond solid-state lasers using Nd^{3+}-doped mixed scandium garnets," J. Opt. Soc. Am. B **10**(8), 1436–1442 (1993).
5. A. Agnesi, S. Dell'Acqua, A. Guandalini, G. Reali, F. Cornacchia, A. Toncelli, M. Toncelli, K. Shimamura, and T. Fukuda, "Optical spectroscopy and diode-pumped laser performance of Nd^{3+} in the CNGG crystal," IEEE J. Quantum Electron. **37**(2), 304–313 (2001).
6. Z. B. Shi, X. Fang, H. J. Zhang, Z. P. Wang, J. Y. Wang, H. H. Yu, Y. G. Yu, X. T. Tao, and M. H. Jiang, "Continuous-wave laser operation at 1.33 μm of Nd:CNGG and Nd:CLNGG crystals," Laser Phys. Lett. **5**(3), 177–180 (2008).
7. H. R. Verdun and L. M. Thomas, "Nd:$CaYAlO_4$ – a new crystal for solid-state lasers emitting at 1.08 μm," Appl. Phys. Lett. **56**(7), 608–610 (1990).
8. A. A. Lagatskii, N. V. Kuleshov, V. G. Shcherbitskii, V. F. Kleptsyn, V. P. Mikhailov, V. G. Ostroumov, and G. Huber, "Lasing characteristics of a diode-pumped Nd^{3+}:$CaGdAlO_4$ crystal," Quantum Electron. **27**(1), 15–17 (1997).
9. C. Feng, H. N. Zhang, Q. P. Wang, and J. X. Fang, "Dual-wavelength synchronously mode-locked laser of a Nd:$Y_3ScAl_4O_{12}$ disordered crystal," Laser Phys. Lett. **14**(4), 045804 (2017).
10. A. A. Kaminskii, V. A. Karasev, V. D. Dubrov, V. P. Yakunin, B. V. Mill', and A. V. Butashin, "New disordered $Ca_2Ga_2SiO_7$:Nd^{3+} crystal for high-power solid-state lasers," Quantum Electron. **22**(2), 97–98 (1992).
11. K. S. Bagdasarov, L. M. Dorozhkin, A. M. Kevorkov, Y. I. Krasilov, A. V. Potemkin, A. V. Shestakov, and I. I. Kuratev, "Continuous lasing in $La_{1-x}Nd_xMgAl_{11}O_{19}$ crystas," Quantum Electron. **13**(5), 639–640 (1983).
12. O. Musset, L. Fouquin, and J. P. Boquillon, "Laser emission under flashlamp pumping of a new crystal: Nd-doped strontium-lanthanum-aluminate (Nd:ASL)," Appl. Phys. B **68**(2), 181–185 (1999).
13. A. V. Terentiev, P. V. Prokoshin, K. V. Yumashev, and V. P. Mikhailov, "Passive mode locking of a Nd^{3+}:$SrLaGa_3O_7$ laser," Appl. Phys. Lett. **67**(17), 2442–2444 (1995).
14. Z. B. Pan, H. J. Cong, H. H. Yu, L. Tian, H. Yuan, H. Q. Cai, H. J. Zhang, H. Huang, J. Y. Wang, Q. Wang, Z. Y. Wei, and Z. G. Zhang, "Growth, thermal properties and laser operation of Nd:Ca3La2(BO3)4: A new disordered laser crystal," Opt. Express **21**(5), 6091–6100 (2013).
15. T. Gbehi, J. Thery, D. Vivien, R. Collongues, G. Dhalenne, and Revcolevschi, "Neodymium sites in Calcium Lanthanide Hexaaluminates, potential laser materials," J. Solid State Chem. **77**(2), 211–222 (1988).
16. S. Alablanche, A. Kahn-Harari, J. Thery, B. Viana, and D. Vivien, "Structural and optical properties of Calcium Neodymium Hexaaluminates single crystals, potential laser materials," J. Solid State Chem. **98**(1), 105–120 (1992).
17. Y. X. Pan, S. D. Zhou, J. W. Wang, B. Xu, J. Liu, Q. S. Song, J. Xu, D. Z. Li, P. Liu, X. D. Xu, and J. Xu, "Growth, spectral properties, and diode-pumped laser operation of a Nd^{3+}-doped $LaMgAl_{11}O_{19}$ crystal," Appl. Opt. **57**(32), 9657–9661 (2018).
18. L. H. Zheng, P. Loiseau, and G. Aka, "Diode-pumped laser operation at 1053 and 900 nm in $Sr_{1-x}La_{x-y}Nd_yMg_xAl_{12-x}O_{19}$ (Nd:ASL) single crystal," Laser Phys. **23**(9), 095802 (2013).
19. J. Q. Di, X. H. Sun, X. D. Xu, C. T. Xia, Q. L. Sai, H. H. Yu, Y. C. Wang, L. Zhu, Y. Gao, and X. Y. Guo, "Growth and spectral characters of Nd:$CaGdAlO_4$ crystal," Eur. Phys. J.: Appl. Phys. **74**(1), 10501 (2016).
20. D. Z. Li, X. D. Xu, S. S. Cheng, D. H. Zhou, F. Wu, Z. W. Zhao, C. T. Xia, J. Xu, H. M. Zhu, and X. Y. Chen, "Polarized spectral properties of Nd^{3+} ions in $CaYAlO_4$ crystal," Appl. Phys. B **101**(1-2), 199–205 (2010).
21. B. R. Judd, "Optical absorption intensities of rare-earth ions," Phys. Rev. **127**(3), 750–761 (1962).
22. G. S. Ofelt, "Intensities of crystal spectra of rare-earth ions," J. Chem. Phys. **37**(3), 511–520 (1962).
23. A. A. Kaminskii, G. Boulon, M. Buoncristiani, B. Di Bartolo, A. Kornienko, and V. Mironov, "Spectroscopy of a new laser garnet $Lu_3Sc_2Ga_3O_{12}$:Nd^{3+}. Intensity luminescence characteristics, stimulated emission, and full set of squared reduced-matrix elements $|\langle\|U^{(t)}\|\rangle|$ for Nd^{3+} ions," Phys. Stat. Sol. (a) **141**(2), 471–494 (1994).
24. X. Y. Chen, Z. D. Luo, D. Jaque, J. J. Romero, J. G. Sole, Y. D. Huang, A. D. Jiang, and C. Y. Tu, "Comparion of opticsl spectra of Nd^{3+} in $NdAl_3(BO_3)_4$ (NAB), Nd:$GdAl_3(BO_3)_4$ (NGAB) and Nd:$Gd_{0.2}Y_{0.8}Al_3(BO_3)_4$ (NGYAB) crystals," J. Phys.: Condens. Matter **13**(5), 1171–1178 (2001).
25. W. T. Carnall, P. R. Fields, and K. Rajnak, "Energy levels in the Trivalent Lanthanide Aqua Ions. I. Pr^{3+}, Nd^{3+}, Pm^{3+}, Sm^{3+}, Dy^{3+}, Ho^{3+}, Er^{3+}, and Tm^{3+}," J. Chem. Phys. **49**(10), 4424–4442 (1968).
26. J. Dong, A. Rapaport, M. Bass, F. Szipocs, and K. Ueda, "Temperature-dependent stimulated emission cross section and concentration quenching in highly doped Nd^{3+}:YAG crystals," Phys. Stat. Sol. (a) **202**(13), 2565–2573 (2005).
27. S. R. Zhao, H. J. Zhang, Y. B. Lu, J. H. Liu, J. Y. Wang, X. G. Xu, H. R. Xia, and M. H. Jiang, "Spectroscopic characterization and laser performance of Nd:$LuVO_4$ single crystal," Opt. Mater. **28**(8-9), 950–955 (2006).
28. C. Y. Shen, D. L. Wang, H. H. Xu, Z. B. Pan, H. J. Zhang, J. Y. Wang, and R. I. Boughton, "Bulk crystal growth and thermal, spectroscopic and laser properties of disordered Melilite Nd:$Ca_2Ga_2SiO_7$ single crystal," J. Alloys Compd. **727**, 8–13 (2017).
29. W. F. Krupke, "Optical absorption and fluorescence intensities in several rare-earth-doped Y_2O_3 and LaF_3 single crystals," Phys. Rev. **145**(1), 325–337 (1966).

Optical Materials EXPRESS

30. Y. Cheng, X. D. Xu, J. Xu, Z. Xin, and S. M. Zhou, "Spectroscopic properties of Nd^{3+}:$CaNb_2O_6$ crystal," Appl. Phys. B **96**(1), 43–50 (2009).
31. N. Li, Y. Y. Xue, D. H. Wang, B. Liu, C. Guo, Q. S. Song, X. D. Xu, J. F. Liu, D. Z. Li, J. Xu, Z. A. Xu, and J. Y. Xu, "Optical properties of Nd:$Bi_4Ge_3O_{12}$ crystals grown by the micro-pulling-down method," J. Lumin. **206**, 412–416 (2019).
32. S. J. Ding, F. Peng, Q. L. Zhang, J. Q. Luo, W. P. Liu, D. L. Sun, R. Q. Dou, J. Y. Gao, G. H. Sun, and M. J. Cheng, "Crystal growth, spectral properties, and continuous wave laser operation of Nd:$GdNbO_4$," J. Alloys Compd. **693**, 339–343 (2017).
33. B. Aull and H. Jenssen, "Vibronic interactions in Nd:YAG resulting in nonreciprocity of absorption and stimulated emission cross sections," IEEE J. Quantum Electron. **18**(5), 925–930 (1982).
34. F. Cornacchia, A. Toncelli, M. Tonelli, E. Cavalli, E. Bovero, and N. Magnani, "Optical spectroscopy of $SrWO_4$:Nd^{3+} single crystals," J. Phys.: Condens. Matter **16**(39), 6867–6876 (2004).
35. H. R. Yang, D. Y. Shen, S. C. Tam, Y. L. Lam, J. G. Liu, K. Ueda, W. J. Xie, and J. H. Gu, "Femtosecond self-mode-locked $La_{1-x}MgNd_xAl_{11}O_{19}$ laser pumped by a laser diode," Jpn. J. Appl. Phys. **39**(Part 1, No. 12A), 6542–6545 (2000).
36. Y. Y. Zhang, H. J. Zhang, H. H. Yu, S. Q. Sun, J. Y. Wang, and M. H. Jiang, "Characterization of disordered melilite Nd:$SrLaGa_3O_7$ crystal," IEEE J. Quantum Electron. **47**(12), 1506–1513 (2011).
37. S. Singh, R. G. Smith, and L. G. Van Uitert, "Stimulated-emission cross section and fluorescent quantum efficiency of Nd^{3+} in yttrium aluminum garnet at room temperature," Phys. Rev. B **10**(6), 2566–2572 (1974).
38. Y. Sato and T. Taira, "Comparative study on the spectroscopic properties of Nd:$GdVO_4$ and Nd:YVO_4 with hybrid process," IEEE J. Sel. Top. Quantum Electron. **11**(3), 613–620 (2005).